Non-Diffusive Momentum Transport and Intrinsic Rotation in Tokamaks

W. X. Wang,[1] S. Ethier,[1] S. Klasky,[2] M. Adams,[3] T. S. Hahm,[1] G. Rewoldt,[1] W. W. Lee,[1] W. M. Tang,[1] and P. H. Diamond[4]

[1]Princeton Plasma Physics Laboratory, P.O. Box 451, Princeton, New Jersey 08543
[2]Oak Ridge National Laboratory
[3]Columbia University
[4]University of California, San Diego

Email: wwang@pppl.gov

Abstract. This paper focuses on using state-of-art gyrokinetic simulations which exploit high performance computational resources to understand toroidal momentum transport and flow generation, which are complex transport phenomena of great importance in magnetic confinement fusion. Critical issues addressed are closely coupled to experimental and theoretical studies with emphasis on electron transport dominated regimes. The key results of our simulations include the identification of nonlinear flow generation by the residual stress (a non-diffusive element of the momentum flux) produced by electrostatic turbulence of ion temperature gradient (ITG) modes and trapped electron modes (TEM). This residual stress is shown to drive intrinsic rotation as a type of wave driven flow phenomenon which operates via wave-particle momentum exchange. The characteristic dependence of non-diffusive momentum transport has been studied over a wide range of experimentally-relevant parameters for the purpose of developing predictive capability for plasma rotation in ITER. Specifically, the "intrinsic" torque associated with residual stress is shown to increase close to linearly with the plasma pressure gradient and the inverse of the plasma current in various turbulence regimes. These results are consistent with experimental trends observed in various toroidal devices. Highlighted results also include robust radial pinches driven by CTEM turbulence, which are shown to play remarkable roles in determining plasma transport. Particularly, the "flow pinch" result from simulations amazingly reproduces the experimental phenomenon of radially inward penetration of perturbed flows created by modulated beams in peripheral regions, and thus is highly illuminating. Also discussed are experimental tests proposed to validate simulation predictions.

1. Introduction

Momentum transport and plasma flow generation are complex transport phenomena of great importance in magnetic confinement fusion. An optimized plasma flow is believed to play a critical role in both controlling macroscopic plasma stability, and in reducing energy loss due to plasma microturbulence. On the other hand, toroidal momentum transport is observed to be highly anomalous, non-diffusive and non-local in nearly all machines. A striking phenomenon found in experiments is the intrinsic or spontaneous rotation; namely, toroidal plasmas can self-organize and develop rotation without an external torque [1]. In fact, the intrinsic rotation in fusion plasmas is an example of a "negative viscosity phenomenon" in which an up-gradient component of the momentum flux organizes

a structured mean flow. Negative viscosity phenomena are of broad interest in the context of atmospheres, oceans, stellar interiors, and other rotating fluids. In current fusion experiments, a large plasma rotation can be driven by neutral beam injection which also provides momentum input while heating the plasma. In large size burning plasmas, however, the use of neutral beams for plasma heating becomes very challenging. It is expected that intrinsic rotation will dominate in future burning plasma experiments. Therefore, understanding the non-diffusive momentum transport mechanisms and the intrinsic rotation phenomenon is a key to predicting plasma flow in ITER.

Recently, extensive experimental studies have been carried out on this topic. The parametric dependence of the intrinsic rotation has been statistically characterized using a broad range of experimental data bases obtained in multiple machines. Specifically, the increment of central intrinsic rotation is shown to increase with the increment of plasma stored energy and to scale with the inverse of the plasma current [2] (the so called Rice scaling). Similar empirical scaling is also observed in other devices including JT-60U [3] and LHD [4], where the intrinsic rotation velocity is shown to increase with the ion pressure gradient in core plasma with an internal transport barrier. There is no doubt that these results are important for making a qualitative projection of plasma rotation in ITER. A more fundamental, critical issue is to understand the underlying physical origins of the experimental empirical scalings. This is the major focus of this study.

Out of various possibilities of physical dynamics which may play roles in determining toroidal rotation, the strong coupling between toroidal momentum and energy transport generally observed in fusion experiments [5] suggests that micro-turbulence is a key player. For turbulence driven toroidal momentum flux, a generic structure can be expressed as follows:

$$\Gamma_\phi \propto -\chi_\phi \frac{\partial U_\phi}{\partial r} + V_p U_\phi + \Pi^{\mathrm{rs}}_{r,\phi}.$$

In addition to diffusion (first term), there are two nondiffusive components, momentum pinch (second term) and residual stress (third term). The three components in the momentum flux are highly distinctive not only formally but also physically. Besides their different physical origins under turbulence circumstances, they have qualitatively distinct effects on the toroidal flow formation. The diffusive transport is well known in the direction opposite to the rotation gradient, leading to the relaxation of the rotation profile and the release of associated free energy. The momentum pinch term is a convective flux which is directly proportional to the rotation velocity U_ϕ with V_p as the pinch velocity. Both momentum diffusion and pinch can move plasma mechanical momentum (i.e., toroidal momentum carried by particles), and then rearrange the rotation profile, radially. A qualitative distinction is that momentum pinch can transport momentum in either direction, up-gradient or down-gradient.

The residual stress $\Pi^{\mathrm{rs}}_{r,\phi}$, which is defined as a specific part of the Reynolds stress with no direct dependence on either the rotation velocity or its gradient, can be shown in the momentum transport equation to be isomorphic in mathematical form to the integrated external momentum source which acts as a torque to drive the rotation. Thus, the residual stress can act as an internal local torque to spin up a plasma, offering an ideal mechanism to drive intrinsic rotation under appropriate boundary conditions. For this reason, the quantity $\nabla\cdot\mathbf{\Pi}^{\mathrm{rs}}_{r,\varphi}$ is widely referred to as the intrinsic torque in experimental and theoretical investigations. In a broad physical context, this is a type of wave-driven flow phenomenon which operates via wave-particle momentum exchange [6]. Note that all three components have been observed in tokamak experiments. Searching for nondiffusive elements and understanding underlying mechanisms have been the focus of recent intensive theoretical and experimental efforts.

In this paper, new results of non-diffusive toroidal momentum transport found from our global gyrokinetic simulations are reported. We focus our study on understanding the nonlinear residual stress generation and its effect on toroidal flow formation in electrostatic turbulence regimes of ion

temperature gradient (ITG) modes and trapped electron modes (TEM). This study concerns a few critical issues which are highly relevant to experimental observations and theoretical studies.

2. Gyrokinetic Simulation Models of Rotation Plasma and Treatment of Kinetic Electrons

In this work, turbulence-driven non-diffusive momentum transport is investigated using the global Gyrokinetic Tokamak Simulation (GTS) code [7] with emphasis on the characteristic dependence of turbulence driven intrinsic rotation on plasma parameters. The GTS code is based on a generalized gyrokinetic simulation model using a δf particle-in-cell approach, and incorporates the comprehensive influence of non-circular cross section, realistic plasma profiles, plasma rotation, neoclassical (equilibrium) electric field, Coulomb collisions, and other features. It can directly read plasma profiles of temperature, density and toroidal angular velocity from the TRANSP experimental database, and a numerical magnetohydrodynamic (MHD) equilibrium reconstructed by MHD codes using TRANSP radial profiles of the total pressure and the parallel current (or safety factor), along with the plasma boundary shape.

First, we give a brief description on our gyrokinetic simulation model for rotating plasmas in this section. In a δf simulation, the turbulence fluctuations are considered as perturbations on the top of the neoclassical equilibrium. The gyrokinetic particle distribution function is expressed as $f = f_0 + \delta f$. The equilibrium distribution function f_0 of ions, with magnetic moment μ and parallel velocity $v_{\|}$ as independent velocity variables, is determined by the neoclassical dynamics and obeys

$$\frac{\partial f_0}{\partial t} + (v_{\|}\hat{b} + \mathbf{v}_{E_0} + \mathbf{v}_d)\cdot\nabla f_0 - \hat{\mathbf{b}}^*\cdot\nabla(\mu B + \frac{e}{m_i}\Phi_0)\frac{\partial f_0}{\partial v_{\|}} = C_i(f_0, f_0). \tag{1}$$

Here, $\mathbf{v}_{E_0}$ is the magnetic drift velocity corresponding to the equilibrium potential Φ_0. $\mathbf{v}_d$ is the ∇B drift velocity, $\hat{\mathbf{b}}^* = \hat{\mathbf{b}} + \rho_{\|}\,\hat{\mathbf{b}}\times(\hat{\mathbf{b}}\cdot\nabla\hat{\mathbf{b}})$ with $\hat{\mathbf{b}} = \mathbf{B}/B$, C_i is the Coulomb collision operator, and e and m_i are the ion charge and mass, respectively. The lowest order solution of Eq. (1) is a shifted Maxwellian consistent with (large) plasma rotation [8]:

$$f_0 = f_{SM} = n(r,\theta)(\frac{m_i}{2\pi T_i})^{3/2} e^{-\frac{m_i}{T_i}[\frac{1}{2}(v_{\|}-U_i)^2+\mu B]}, \tag{2}$$

where the parallel flow velocity U_i is associated with the toroidal rotation by $U_i = I\omega_\phi/B$ with ω_ϕ the toroidal angular velocity and I the toroidal current, and $n_i(r, \theta)$ is the ion density, $n_i(r,\theta) = N(r)e^{\frac{m_i U_i^2}{2T_i} - \frac{e\tilde{\Phi}_0}{T_i}}$, with poloidal variation associated with plasma rotation. The total equilibrium potential consists of two parts, $\Phi_0 = \langle\Phi_0\rangle + \tilde{\Phi}_0$. Here, $\langle\ \rangle$ denotes a flux surface average. The poloidally varying component $\tilde{\Phi}_0$ can be generated by the centrifugal force which drives charge separation on a magnetic surface in strongly rotating plasmas [9]. Generally the radial potential $\langle\Phi_0\rangle$ is dominant. The equilibrium radial electric field can be calculated from a first-principles based particle simulation of neoclassical dynamics with important finite orbit effects [8], or obtained by direct experimental measurement if available. Instead of using a true neoclassical equilibrium distribution function, which is unknown analytically, we use this lowest order solution for equilibrium toroidal plasmas in the present simulations. A shifted Maxwellian with either model or experimental profiles of $\langle n(r,\theta)\rangle$, $T_i(r)$ and $\omega_\phi(r)$ is prescribed for the ions. In the electrostatic limit, the ion gyrokinetic equation for the turbulence perturbed distribution δf_i of ion guiding centers is

$$\frac{\partial \delta f_i}{\partial t} + (v_\parallel \hat{b} + \mathbf{v}_{E_0} + \mathbf{v}_E + \mathbf{v}_d) \cdot \nabla \delta f_i - \hat{\mathbf{b}^*} \cdot \nabla(\mu B + \frac{e}{m_i}\Phi_0 + \frac{e}{m_i}\bar{\Phi})\frac{\partial \delta f_i}{\partial v_\parallel} =$$

$$\Big\{ - \left[\frac{m}{T_i}\left(\frac{1}{2}(v_\parallel - U_i)^2 + \mu B\right) - \frac{3}{2}\right] \mathbf{v}_E \cdot \nabla \ln T - \mathbf{v}_E \cdot \nabla \ln n(r,\theta) - \frac{m(v_\parallel - U_i)}{T_i}\mathbf{v}_E \cdot \nabla U_i(r,\theta)$$

$$+ \frac{mU_i}{T_i v_\parallel}\mathbf{v}_E \cdot \mu \nabla B - \frac{1}{T_i}(v_\parallel \hat{b} + \mathbf{v}_d) \cdot \nabla(e\bar{\Phi})(1 - \frac{U_i}{v_\parallel})\Big\} f_0 + C_i^l(\delta f_i). \tag{3}$$

Here, $\mathbf{v}_E$ is the $\mathbf{E} \times \mathbf{B}$ velocity corresponding to the fluctuation potential $\bar{\Phi}(\mathbf{R})$ at the ion guiding center coordinates $\mathbf{R}$, and C_i^l is the linearized Coulomb collision operator. On the right hand side, the third term proportional to ∇U_i is the Kelvin-Helmholtz-type drive term. The other terms containing U_i are also retained, which can be important when the Mach number of plasma flow is high.

The GTS code solves the gyrokinetic Poisson equation in configuration space for the turbulence potential $\Phi(\mathbf{x})$ at the particle coordinates $\mathbf{x}$. Unlike in flux-tube or wedge codes, the real space, global Poisson solver, in principle, retains all toroidal modes from (m/n =0/0) all the way to a limit which is set by grid resolution, and therefore retains full-channel nonlinear energy couplings. There are two largely different Poisson solvers implemented in the GTS simulation. In a simple geometry limit, i.e., large aspect ratio and circular cross section, turbulence fluctuations $\delta\Phi$ on small spatial and fast time scales and axisymmetric zonal flow $\langle\Phi\rangle$ on larger (meso-scale) spatial and slow time scales can be decoupled using i) a Pade approximation, i.e., $\Gamma_0(b) \equiv I_0(b)e^{-b} \approx 1/(1 + b)$ with I_0 the modified Bessel function and $b = (k_\perp\rho_i)^2$, and ii) $\langle\tilde{\Phi}\rangle \approx \langle\widetilde{\Phi}\rangle$, , i.e., operations between the flux surface average $\langle\Phi\rangle$ and the gyrokinetic double average $\tilde{\Phi}$ can commute. This results in two decoupled equations [7]:

$$\frac{e}{T_i}\left(\delta\Phi - \widetilde{\delta\Phi}\right) = \frac{\delta\bar{n}_i - \langle\delta\bar{n}_i\rangle}{n_0} - \frac{\delta n_e - \langle\delta n_e\rangle}{n_0}, \tag{4}$$

$$\frac{1}{\mathcal{V}_r'}\frac{d}{dr}\left[\frac{d\langle\Phi\rangle}{dr}\mathcal{V}_r'\langle g^{rr}\rangle\right] = \frac{1}{\mathcal{V}_r'}\frac{d}{dr}\left\{\frac{d}{dr}\left[\frac{T_i}{e}\left(\frac{\langle\delta\bar{n}_i\rangle}{n_0} - \frac{\langle\delta n_e\rangle}{n_0}\right)\right]\mathcal{V}_r'\langle g^{rr}\rangle\right\}$$
$$-\langle\frac{1}{\rho_i^2}\rangle\frac{T_i}{e}\left(\frac{\langle\delta\bar{n}_i\rangle}{n_0} - \frac{\langle\delta n_e\rangle}{n_0}\right), \tag{5}$$

where $\delta\bar{n}_i(\mathbf{x})$ and $\delta n_e(\mathbf{x})$ are the ion and electron density fluctuations, respectively, $\mathcal{V}_r' \equiv d\mathcal{V}/dr$, with $\mathcal{V}$ the volume enclosed by magnetic surface r, and $g^{rr} \equiv \nabla r \cdot \nabla r$. Because turbulence dynamics on different spatio-temporal scales are separated in solving the Poisson equation, the advantages are apparent. However, the above approximations, particular the second one, are not well justified in general toroidal geometry. This has motivated us to develop a generalized Poisson solver which solves an integral equation for the total potential $\Phi = \delta\Phi + \langle\Phi\rangle$,

$$\frac{e}{T_i}\left(\Phi - \widetilde{\Phi}\right) = \frac{\delta\bar{n}_i}{n_0} - \frac{\delta n_e}{n_0}. \tag{6}$$

While the adiabatic electron model has been widely used for simplicity in many earlier numerical and theoretical studies of ITG driven turbulence, non-adiabatic electron physics is in general irreducible in turbulence dynamics of toroidal systems. For ITG and TEM turbulence with $k_\perp\rho_e \ll 1$, we use a drift kinetic description for electrons, neglecting the finite gyroradius effect. However, for

electron gyroradius scale turbulence, such as electron temperature gradient driven turbulence, electrons are treated as fully gyrokinetic. Similarly as for ions, the δf method can be used to solve for the total perturbed electron guiding center distribution function, $\delta f_e = f_e - f_{e0}$, corresponding to turbulence fluctuations. The equilibrium distribution f_{e0} satisfies the electron version of Eq. (1) and can be approximated by a shifted Maxwellian containing a parallel flow similar to that for the ions. Apparently, δf_e contains both adiabatic and non-adiabatic electron response. Another simulation model to treat kinetic electrons is to separate the non-adiabatic electron response δh_e using $f_e = f_{e0} + (e\delta\Phi/T_e)\, f_{e0} + \delta h_e$, and to solve for the non-adiabatic part δh_e according to Eq. (16) of Ref. 7. In this case, Eq. (4) becomes

$$\left(1+\frac{T_i}{T_e}\right)\frac{e\delta\Phi}{T_i} - \frac{e\widetilde{\delta\Phi}}{T_i} = \frac{\delta\bar{n}_i - \langle\delta\bar{n}_i\rangle}{n_0} - \frac{\delta n_e^h - \langle\delta n_e^h\rangle}{n_0}, \tag{7}$$

and Eq. (6) becomes

$$\left(1+\frac{T_i}{T_e}\right)\frac{e\Phi}{T_i} - \frac{e\widetilde{\Phi}}{T_i} - \frac{e\langle\Phi\rangle}{T_e} = \frac{\delta\bar{n}_i}{n_0} - \frac{\delta n_e^h}{n_0}, \tag{8}$$

where $\delta n_e^h \equiv \int d^3v\,\delta h_e$ is the non-adiabatic electron density fluctuation.

The left-hand side of the δh_e equation (Eq. (16) of Ref. 7) contains a time derivative term, $\frac{\partial\delta\Phi}{\partial t}$, which can easily give rise to numerical instability if it is calculated using direct finite differences. To avoid the numerical problem, a split-weight scheme [10] was proposed, which uses a separate equation for calculating $\frac{\partial\Phi}{\partial t}$. The $\frac{\partial\Phi}{\partial t}$ equation, which is not a new equation, is obtained by taking the time derivative of the gyrokinetic Poisson equation and using the ion and electron continuity equations. In a toroidal system, the equation for calculating $\frac{\partial\Phi}{\partial t}$ is obtained as follows:

$$\frac{e}{T_i}\left(\frac{\partial\Phi}{\partial t} - \widetilde{\frac{\partial\Phi}{\partial t}}\right) = \frac{1}{n_0}(\nabla\cdot\mathbf{\Gamma}_e - \nabla\cdot\mathbf{\Gamma}_i) + \frac{c\mathbf{B}\times\nabla\delta\Phi}{B^2}\cdot\left(2\frac{\nabla B}{B} - \frac{e}{T_e}\nabla\Phi_0\right), \tag{9}$$

where wide-tilde denotes the gyrokinetic double average over $\frac{\partial\Phi}{\partial t}$, electron particle flux $\mathbf{\Gamma}_e \equiv \int d^3v(v_\parallel\mathbf{b} + \mathbf{v}_{E_0} + \mathbf{v}_E + \mathbf{v}_d)\delta h_e$ and ion particle flux $\mathbf{\Gamma}_i \equiv (1/2\pi)\int d^3v d\mathbf{R} d\Theta\, (v_\parallel\mathbf{b} + \mathbf{v}_{E_0} + \mathbf{v}_E + \mathbf{v}_d)\delta f_i \delta(\mathbf{R} - \mathbf{x} + \rho)$, with ρ the gyroradius vector and Θ the gyrophase. Then $\frac{\partial\delta\Phi}{\partial t}$ is calculated directly using $\frac{\partial\delta\Phi}{\partial t} \equiv \frac{\partial\Phi}{\partial t} - \left\langle\frac{\partial\Phi}{\partial t}\right\rangle$.

It is noticed that many previous simulations include only trapped electrons for the non-adiabatic electron response. Numerically, the fast parallel streaming of passing electrons gives rise to a strict constraint on the time step size, which adds to the computational challenge. While the trapped electrons are the primary origin of non-adiabatic response, some passing electrons can be non-adiabatic too. In fact, dynamical division between trapped and passing electrons is, though not impossible, highly non-trivial during simulations because of the dependence of the trapping-passing boundary on the electric potential which evolves in time, and of the collisional trapping-detrapping process. Nevertheless, thanks to the availability of supercomputing capabilities, we retain full electron dynamics by including both trapped and untrapped electrons in the simulations.

The GTS simulation has been benchmarked against other gyrokinetic codes in the electrostatic regime and the large aspect ratio circular concentric geometry limit [7, 11]. Further verification studies have been carried beyond linear benchmarks. We here present a few examples.

Unlike ITG turbulence with adiabatic electrons, non-adiabatic electron dynamics can drive particle transport for turbulence such as TEM. It is well known that turbulence driven particle transport across the magnetic field lines is ambipolar, i.e., flux-surface-averaged radial particle fluxes for electrons and ions are equal, so as to maintain the overall quasineutrality in a toroidal system. The ambipolarity property of TEM driven cross-field particle transport is tested in the GTS simulation. The time history of particle fluxes (at $r/a = 0.54$) is plotted in Fig. 1, showing that electron and ion fluxes very closely track with each other all the time during the simulation. Moreover, the ambipolarity of turbulence driven particle transport is obtained locally over the entire radial domain ($0.1 \leq r \leq 0.9$) of the global simulation, as is seen in the right panel of Fig. 1 which plots the steady state particle fluxes versus minor radius. This guarantees that quasineutrality is satisfied radially locally.

Global gyrokinetic turbulence is characterized by distinguishable dynamical phases in both coordinate space and wavenumber space [12]. Ideally, the dynamics of gyrokinetic turbulence should be robust to numerical techniques. A convergence study for CTEM turbulence is presented in Fig. 2. Two simulations using 50 and 100 particles/cell species, respectively, are shown to produce well converged results for electron particle transport that displays no noticeable difference in statistical sense (left panel). In other words, the difference in the simulated fluxes between the two cases using 50 and 100 particles/cell·species is within the same range of statistical error of different simulation runs with the same number of particles but with different initial conditions. At the mean time, the time evolution of corresponding average electron weight square, $\langle w^2 \rangle$, of the two simulations is shown to be almost identical (right panel). This result indicates that the observed weight growing does not depend on whether 50 or 100 particles/cell·species are used in these simulations, and is driven by physics, corresponding to the increase of amplitude of δf associated with plasma profile evolution induced by turbulence-driven fluxes during transport time scale. Furthermore, while the particle weight is physically growing during the simulations, there is no observable correlation between the weight evolution and the dynamics of electron particle flux, as is shown in Fig. 2. The particle weight remains at a low level ($\langle w^2 \rangle < 0.09$) at the end of the simulations, which does not impact the results of simulated transport. These convergence studies clearly indicate that the noise-induced transport in our simulations is negligible with respect to turbulence driven transport.

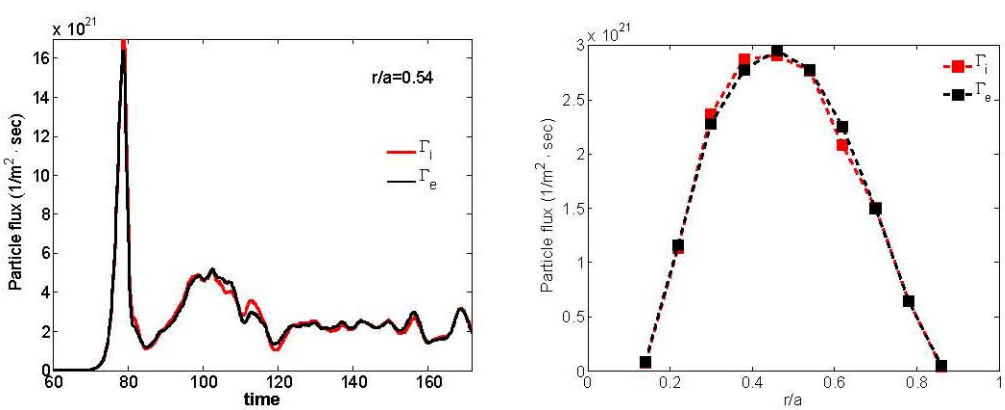

Figure 1. Time history of ion and electron particle fluxes (left), and steady state ion and electron particle fluxes versus minor radius r (right). Time unit is L_n/c_s.

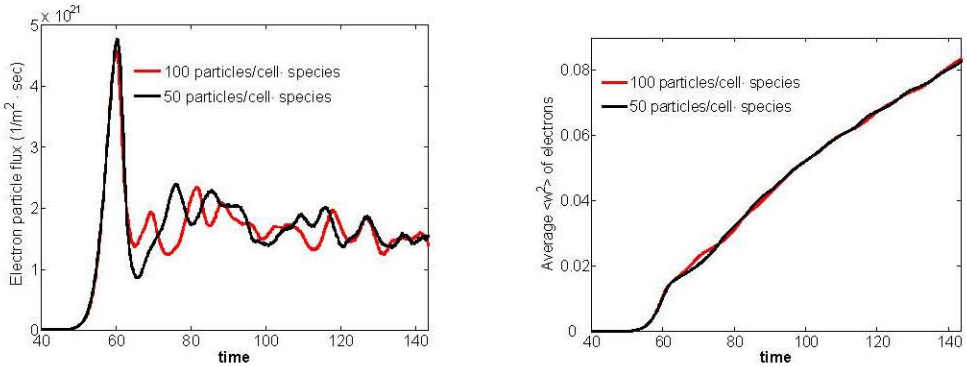

Figure 2. Time history of electron particle fluxes (left), and average weight squares of electrons (right) from two simulations using different number of simulation particle. Time unit is L_{T_e}/c_s. The major parameters used are: $R_0/L_{T_e} = R_0/L_n = 6.5$, $R_0/L_{T_i} = 2.4$. A shaped DIII-D type MHD equilibrium is used.

3. Nonlinear Flow Generation by Gyrokinetic Turbulence

To search for nondiffusive elements of toroidal momentum transport and understand underlying mechanisms, global gyrokinetic simulations using the GTS code have been carried out systematically over a wide range of experimentally relevant parameters. Our simulation studies have revealed an important nonlinear flow generation process due to the residual stress produced by electrostatic ITG and TEM turbulence [11, 13]. Particularly, in collisionless TEM (CTEM) turbulence, both turbulence fluctuation intensity and the intensity gradient are identified as nonlinear mechanisms for driving residual stress. Another key ingredient for turbulence driven residual stress is symmetry breaking in the parallel wave number spectrum. Such a well know mechanism is the mean $\mathbf{E} \times \mathbf{B}$ flow shear [14, 15]. For most drift wave instabilities, both signs of $k_{||}$ are equally excited in the ideal case, resulting in a reflection symmetry in the $k_{||}$ spectrum. Perfect local $k_{||}$ symmetry means perfectly balanced population density between co-and counter-propagating acoustic waves along the torus, and thus a vanishing net local momentum torque. Therefore, a critical, generic piece of physics behind the residual stress spinning up the plasma is the breaking of the $k_{||} \rightarrow -k_{||}$ symmetry. Concerning the origin of the symmetry breaking, turbulence self-generated low frequency zonal flow shear has been identified to be a key, universal mechanism in various turbulence regimes. Simulations also indicate the existence of other mechanisms beyond $\mathbf{E} \times \mathbf{B}$ shear.

Figure 3 illustrates how the residual stress is nonlinearly driven by turbulence intensity, acting with turbulence-generated zonal flow induced $k_{||}$ symmetry breaking. These results are obtained from a simulation of CTEM turbulence, using typical parameters of DIII-D plasmas. The major parameters used here are: $R_0/L_{T_e} = R_0/L_n = 6.0$, $R_0/L_{T_i} = 2.4$, $T_e = 4.8$ Kev and $T_i = 3.5$ Kev at $r/a = 0.5$, and an initial rotation $\omega_\phi = 0$. First, the CTEM-driven toroidal flux exhibits coherent spatio-temporal bursting behavior with momentum flux pulses propagating both inward and outward in the radial direction, as shown in the upper-left panel of Fig. 3. Because of the zero initial toroidal rotation used, the momentum flux is, by definition, essentially residual stress. Interestingly, the residual stress at steady state changes direction from outward in the inner core region to inward in the outer core region. Plotted in the lower-left panel is $\sum k_{||}\delta\Phi_{mn}^2$, where $\delta\Phi_{mn}$ is a mode amplitude, with m and n the poloidal and toroidal mode numbers, respectively. This quantity can be used to measure the component of the residual stress driven by the turbulence intensity in the presence of non-vanishing $\langle k_{||} \rangle$. One can see that $\sum k_{||}\delta\Phi_{mn}^2$ indeed reproduces a similar spatio-temporal behavior to the directly calculated momentum flux, particularly in the inner core region ($r/a < 0.55$). In the

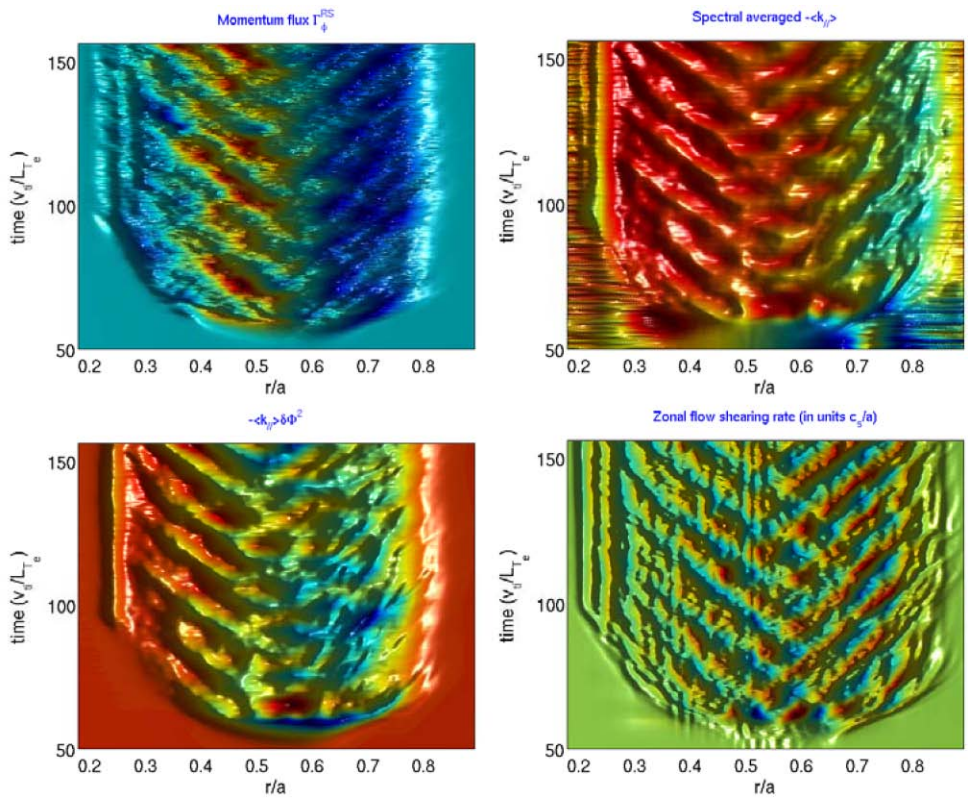

Figure 3. Spatio-temporal evolution of radial flux of toroidal momentum (upper-left), $\langle k_{||}\rangle \sum \delta\Phi_{mn}^2$ (lower-left), spectrum-averaged $\langle k_{||}\rangle$ (upper-right), zonal flow shearing rate (lower right).

outer core region (r/a > 0.55), the turbulence intensity gradient is identified to play significant role in driving residual stress [11]. Further, in the upper-right panel, the spectrum-averaged $k_{||}$, defined as

$$\langle k_{||}\rangle(r) \equiv \frac{1}{qR_0}\frac{\sum(n/|n|)(nq-m)\delta\Phi_{mn}^2}{\sum \delta\Phi_{mn}^2},$$

shows an apparent spatio-temporal correlation with $\Gamma_\phi^{\mathrm{RS}}$, indicating the importance of nonvanishing $\langle k_{||}\rangle$. The whole picture for the residual stress generation is completed by finding out what causes $k_{||}$ symmetry breaking, giving rise to the non-zero $\langle k_{||}\rangle$. This is in the lower-right panel which plots the shearing rate of turbulence self-generated zonal flows according to the following expression

$$\omega_E^{\mathrm{ZF}} = \frac{R^2 B_p^2}{B}\frac{\partial}{\partial \Psi_p}\left(\frac{E^{\mathrm{ZF}}}{RB_p}\right),$$

where B and B_p are the total and poloidal magnetic field strengths, and Ψ_p is the poloidal magnetic flux. A clear correlation between the zonal flow shearing rate ω_E^{ZF} and $\langle k_{||}\rangle$ indicates that the breaking of $k_{||}$ symmetry and the yielding of nonvanishing $\langle k_{||}\rangle$ are caused by the zonal flow shear. Since zonal flows are turbulence self-generated, this process represents a universal, nonlinear mechanism for residual stress generation.

4. Characteristics of Turbulence-Nonlinearly-Driven Plasma Flow and Origin of Empirical Scalings of Intrinsic Rotation

The turbulence-nonlinearly-driven residual stress, acting as an intrinsic torque, is shown to spin up toroidal rotation effectively. In our previous study, ITG turbulence driven "intrinsic" torque is shown to increase close to linearly with plasma pressure gradient [11], in qualitative agreement with experimental observations in various devices. For typical plasma parameters of fusion experiments, collisionless TEM turbulence can be a major source to drive multiple-channel transport, including toroidal momentum transport. However, the momentum transport and flow generation phenomena have not been well explored experimentally in the electron transport dominated regimes. Quantifying the characteristic dependence of turbulence generated toroidal flow in the electron turbulence regimes is particularly important for ITER experiments in which the electron channel is expected to dominate plasma transport.

The characteristic dependence of intrinsic torque driven by CTEM turbulence is numerically investigated. The GTS simulations are carried out over a wide range of experimentally relevant plasma parameters, which cover various regimes with respect to different sources of free energy for driving CTEM turbulence.

First, we examine the dependence of intrinsic rotation on electron pressure gradient. For this parametric scan study, radial profiles of electron density/temperature/pressure gradient used in simulations are specified according to the expression: $R_0/L_{n_e,T_e,p_e} = -\kappa \exp\left[-\left(\frac{\rho-\rho_c}{0.28}\right)^6\right]$, along with a fixed density/temperature/pressure at the center ρ_c = 0.5. This gives a fairly uniform CTEM drive in a region centered at ρ_c and near zero gradient elsewhere. The simulation scan is performed by varying the κ value. For all these simulations, plasmas are initially rotation-free and momentum-source-free, which allows us to concentrate on the residual stress associated intrinsic torque. An equilibrium $\mathbf{E} \times \mathbf{B}$ shear is also included via the radial force balance relation, which, however, is seen to be a minor player with respect to CTEM self-generated zonal flows. The numerical MHD equilibrium used in this study corresponds to a real DIII-D discharge. All simulations in this paper use 100 particle/cell·species.

Instead of calculating the local torque $\nabla \cdot \mathbf{\Pi}^{\mathrm{RS}}_{r,\phi}$, we examine the rate of toroidal momentum generation, dP_ϕ/dt, associated with the residual stress, with $P_\phi \equiv \int d^3r \left| \int d^3v m_i R v_\phi \delta f_i \right|$. Apparently, the quantity dP_ϕ/dt is a measure of the volume-integrated (or spatially averaged) torque driven by turbulence, which has better correspondence to the intrinsic torque inferred from experiments or measured central intrinsic rotation. The simulation results of total intrinsic torque dP_ϕ/dt driven by CTEM turbulence, versus the electron pressure gradient ∇p_e, are summarized in Fig. 4. The three curves in Fig. 4 correspond to three cases of free energy for driving CTEM. The dominant free energy sources are ∇n (black), ∇T_e (green) and a combination of both (red), respectively. For all three cases, the intrinsic torque associated with nonlinearly generated residual stress is found to increase close to linearly with the electron pressure gradient. In the other words, a larger central intrinsic rotation is expected to be produced in a plasma with a higher electron pressure gradient. The dominant underlying physics governing this scaling is rather straightforward, namely, both the turbulence intensity and the zonal flow shear, which are two key ingredients for driving residual stress, are increased with the strength of the CTEM drive R_0/L_{p_e}. Moreover, the observation of the black curve being above the green and red curves indicates that the free energy in the density gradient is more efficient in driving intrinsic rotation via CTEM turbulence. These results predicted from the gyrokinetic simulations suggest a strong connection between intrinsic rotation and electron parameters. It is highly interesting to test this prediction in experiments. As a good opportunity for validation study, particularly, NSTX experiments can be used as a unique platform to test the

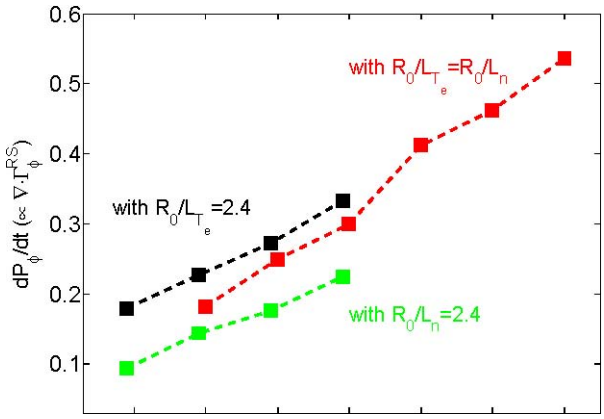

Figure 4. CTEM-driven total intrinsic torque (spatially averaged) versus electron pressure gradient R_0/L_{p_e}.

predicted characteristic dependence of intrinsic rotation on electron parameters in electron transport dominated regimes.

Now we turn to exploring the dependence of residual stress and intrinsic rotation on the plasma current I_p. Again, this simulation study is carried out for CTEM turbulence. The primary purpose is to attempt to shed light on the physics origin of the current scaling which was obtained in multiple devices [2]. For this simulation study we adopt a similar methodology to that used in experiments for various investigations of current scans. A set of simulation experiments is carried out by holding the vacuum (external) magnetic field and plasma pressure profile fixed, while varying the plasma current. Specifically, this is accomplished by generating a series of shaped, numerical equilibria with I_p = 0.75, 1.0, 1.5 and 2.0 MA, using an MHD code.

The major parameters used in this study are: R_0/L_{T_e} = R_0/L_n = 6, R_0/L_{T_i} =2.4 and 100 particles/cell·species. Simulation results presented in the right panel of Fig. 5 show that the rate of toroidal momentum generation by CTEM turbulence (i.e., total intrinsic torque) increases close to linearly with the inverse of the plasma current. This result indeed reproduces the same trend as that of the Rice scaling. With respect to the torque versus ∇T, ∇n and ∇p scaling in the ITG and CTEM turbulence, however, the underlying physics governing the current scaling is less transparent.

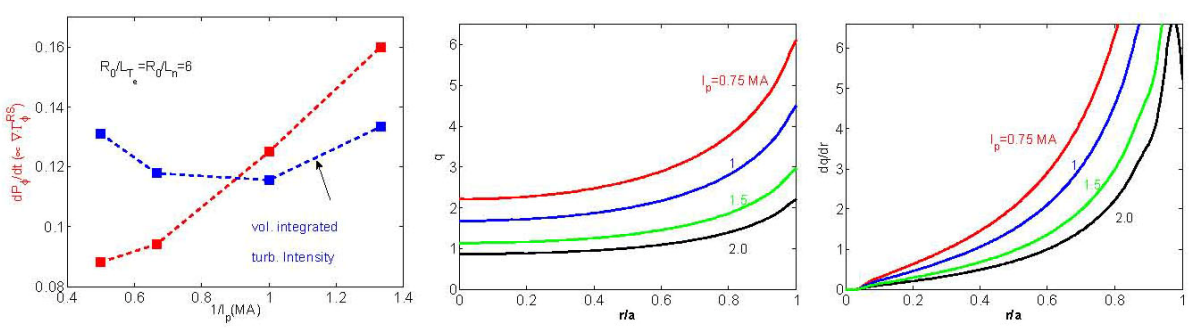

Figure 5. CTEM-driven total intrinsic torque and volume-integrated turbulence intensity at steady state versus plasma current I_p (left), and corresponding radial profiles of safety factor q (middle) and magnetic shear dq/dr (right) of the four cases.

Both turbulence intensities and intensity gradients are shown to drive the residual stress. First, we examine the turbulence intensity levels of four cases. As is also shown in the right panel of Fig. 5, the volume-integrated turbulence intensities in the steady state are actually on the same level for the four cases, roughly independent of the current. At the same time, the turbulence intensity gradient, which

can also contribute to driving residual stress with an asymmetric fluctuation spectrum in $k_{||}$ due to turbulence wave radiation induced wave momentum diffusion [16], also does not show significant current dependence that can account for the torque vs I_p scaling observed in our simulations. Hence, this implies that the underlying physics for the current scaling has to do with the symmetry breaking dynamics and the associated nonvanishing spectrally averaged $k_{||}$. As we found previously, the turbulence self-generated zonal flow shear is a key mechanism for the symmetry breaking. Simulations also indicate the existence of other mechanisms beyond $\mathbf{E} \times \mathbf{B}$ shear. These include the magnetic shear, to be discussed below.

On the other hand, the corresponding q profile is remarkably boosted in the four equilibria as the plasma current is decreased from 2 MA to 0.75 MA, as shown in the middle panel of Fig. 5. So is the magnetic shear dq/dr (left panel of Fig. 5). Note that the parameter $\rho_*(\equiv \rho_i/a)$ for the four cases is roughly the same, i.e., $a/\rho_i \sim 170$, which is in the DIII-D range. This observation is highly suggestive that the current scaling of intrinsic torque and rotation may have connections with the change in the magnetic shear and/or the value of q.

To identify the effects of the safety factor and the magnetic shear separately, further computational experiments are performed. First, we examine the effect of the q value. To this end, three MHD equilibria are created, which hold the profile of magnetic shear (and plasma pressure) fixed while boosting the q profile, as shown in the right panel of Fig. 6. As illustrated in the left panel of Fig. 6, the CTEM driven intrinsic torque is shown to decrease with the increase of the q value for this scan. The dependence of the volume-integrated turbulence intensity on q value plotted in the same figure indicates that this turbulence intensity dependence appears to be a major cause for the observed intrinsic torque vs q dependence. The key point of this interesting result, however, is that the dependence of the torque on the q value shows the opposite trend to the current scaling obtained in Fig. 5. Therefore, the current scaling is not due to the effect of the q value on the nonlinear residual stress generation.

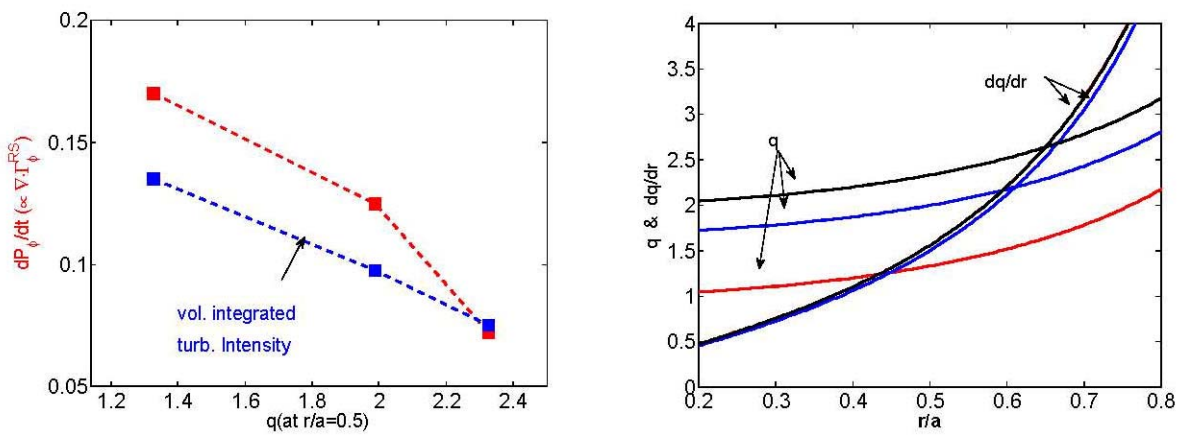

Figure 6. CTEM-driven total intrinsic torque versus q value averaged over the core region (left) and corresponding radial profiles of q and dq/dr for the three equilibria used for these simulations (right).

Now we turn to exploring the effects of the magnetic shear on the intrinsic torque. To this end, three MHD equilibria are created, which hold the radially averaged q value nearly fixed in the central core region where CTEM turbulence is generated, but allow minor variation in the q profile in order to create significant variation in the magnetic shear, as illustrated in the middle and right panels of Fig. 7. At the same time, the plasma pressure is also held fixed. Note that a normal (positive) magnetic shear is presented in these equilibria. The result of this simulation scan is presented in the left panel of Fig. 7, which shows that the volume-integrated intrinsic torque increases nearly linearly with the

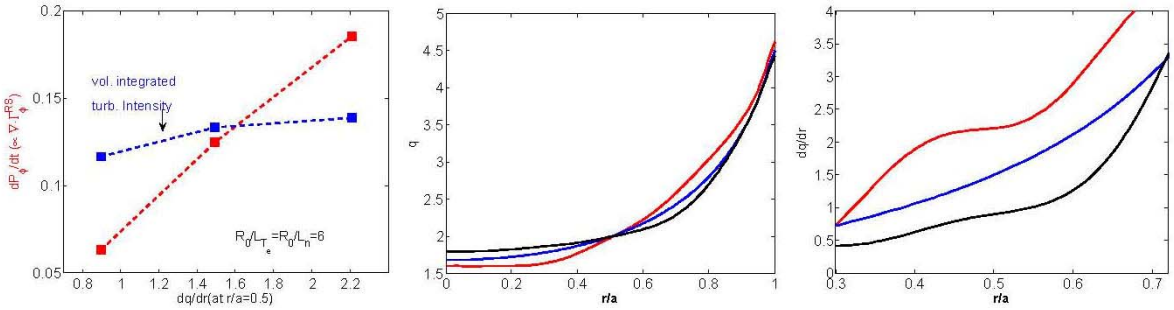

Figure 7. CTEM-driven total intrinsic torque versus magnetic shear averaged over the central core region (left), and corresponding radial profiles of q (middle) and dq/dr (right) of the three equilibria used for these simulations.

magnetic shear. On the other hand, the volume-integrated fluctuation intensity exhibits a much weaker dependence on the magnetic shear, which indicates that the observed intrinsic torque vs the magnetic shear scaling mostly results from the effect of the $k_{||}$ symmetry breaking physics. Specifically, the enhancement of CTEM driven intrinsic torque with magnetic shear is caused by the enhanced $k_{||}$ symmetry breaking due to stronger magnetic shear. The key point of this result is that the dependence of the intrinsic torque on dq/dr indeed produces the right trend which is consistent with the current scaling obtained in Fig. 5. Therefore, given the distinct effects of varying the q value and the magnetic shear on intrinsic torque generation, it is concluded that the current scaling results from the effect of magnetic shear on the turbulence spectrum, namely, the magnetic shear induced $k_{||}$ symmetry breaking, which is enhanced with increased magnetic shear. We should point out that the effect of magnetic shear on the nonlinear residual generation and the associated key role of it behind the current scaling revealed by these gyrokinetic simulations should be tested and validated by experiments. To a certain extent, this can be done by revisiting the experimental data base from which the current scaling was revealed.

For current scan studies, another scenario often adopted in experiments is to hold the q profile and the pressure profile fixed, while varying the current. In this case, the vacuum magnetic field has to change correspondingly, according to $B_{\mathrm{vac}} \propto I_p$. Our nonlinear CTEM simulations have been also carried out to explore the current dependence of intrinsic rotation in this scenario. We used the same simulation parameters as in Fig. 5, except for the MHD equilibria. Simulation results are presented in Fig. 8. In this case, the CTEM driven intrinsic torque is found to increase close to linearly with the vacuum field. It is important to notice that in this scan scenario, the parameter ρ_* for the three cases

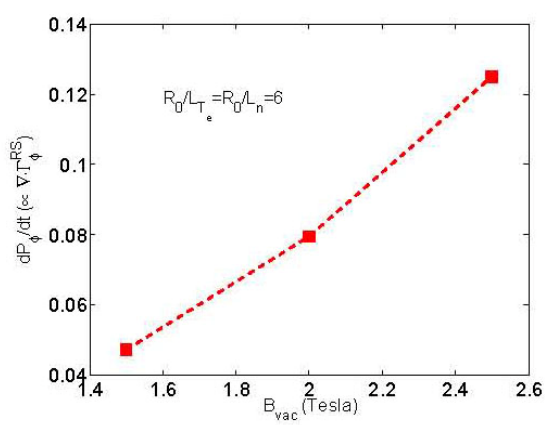

Figure 8. Total intrinsic torque versus external magnetic field B_{vac} in CTEM turbulence.

varies significantly, from $a/\rho_i \sim 130$ for B_{vac} = 1.5 Tesla to $a/\rho_i \sim 230$ for B_{vac} = 2.5 Tesla, which is an important factor impacting turbulence transport. Thus, the variation in ρ_* should be taken into account when we look into the results in Fig. 8 in connection with the experimental scaling. Nevertheless, this current scan scenario is considered to be less relevant to the current scaling obtained in experiments.

5. Meso-scale Phenomena in CTEM Turbulence—Flow, Particle and Heat Pinch and Large Scale Structure Formation

A few highly remarkable, interesting features observed in our CTEM simulations are discussed in this section.

First, nonlinear GTS simulations have found that meso-scale phenomena and associated nonlocal transport are highly pronounced in the TEM turbulence regime, probably because of strong coherent wave-particle interaction at magnetic precession resonances of trapped electrons. Remarkably, the parallel (and toroidal) flow exhibits coherent temporal burstings and radial propagation during its generation process, as is clearly seen in the upper-left panel of Fig. 9. Particularly, it is shown that small parallel flow perturbations are generated locally (in the center of the plasma in the simulation case) by the turbulence, and then propagate radially. The measured propagation velocity is $\sim 7 \times 10^{-3} c_s$ with c_s the sound speed. This "flow pinch" phenomenon observed in the simulations appears to phenomenologically reproduce a well-known experimental result in JT-60U where perturbed flows created by modulated beams were demonstrated to penetrate radially from the peripheral region of the plasma into the core [3]. Thus, it is highly illuminating. Furthermore, radial pinches appear to be a very robust and generic feature in CTEM turbulence, and are found to emerge in all transport channels, including particle, electron heat and ion heat. These are illustrated in Fig. 9. One highly

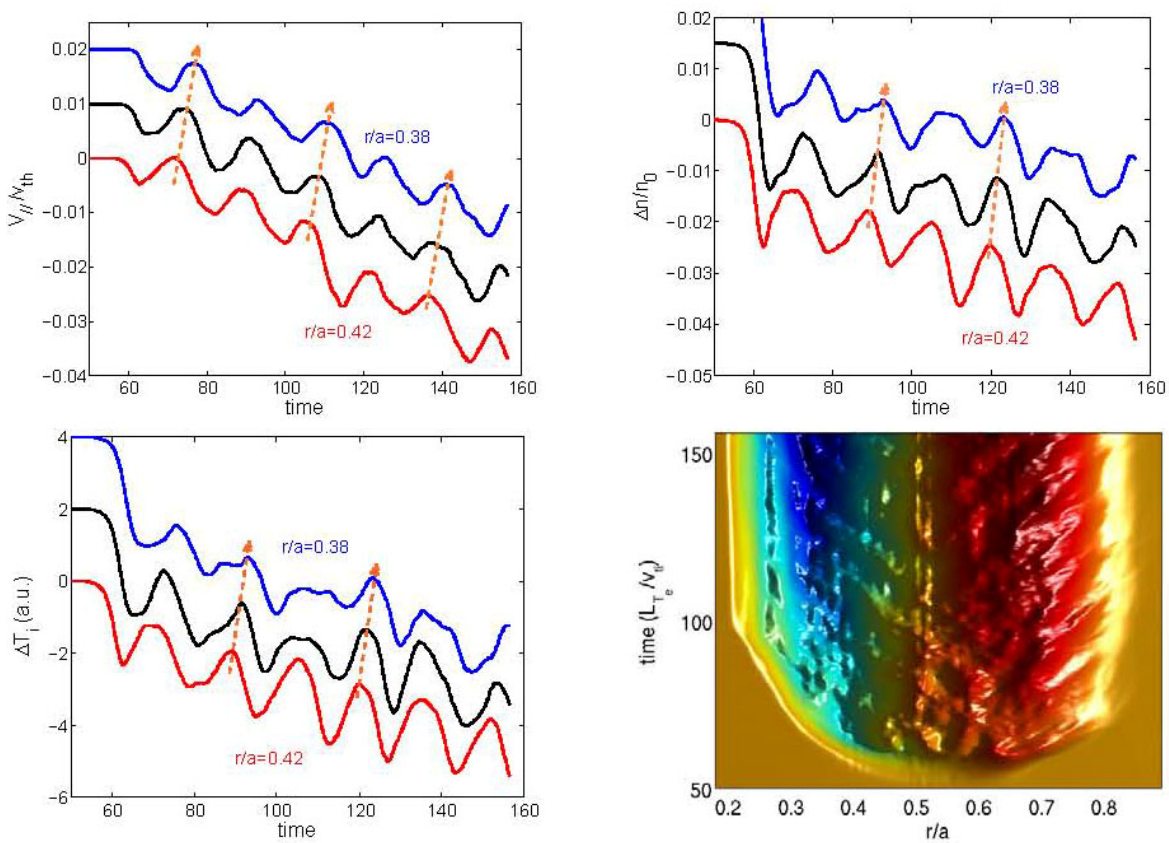

Figure 9. Time history of parallel flow (upper-left), density (upper-right) and ion temperature ΔT_i (lower-left) at three radial locations, and spatio-temporal evolution of electron temperature ΔT_e (lowerright), illustrating generic pinch phenomenon in CTEM turbulence.

remarkable fact found is that the radial pinches in different transport channels emerge “in phase”. We point out that the density pinch and heat pinch carried by electron turbulence as suggested by our nonlinear CTEM simulations can be tested by designing similar perturbative experiments to ones with modulated flows.

Finally, as a remarkable meso-scale phenomena, ∇T_e-driven CTEM turbulence in specific, experimentally relevant parameter regimes is found to generate large fluctuation structures with toroidal mode number $n \lesssim 10$ via dramatic inverse energy cascades, as shown in Fig. 10. This phenomenon may have a natural connection to the generation of blobs widely observed in the tokamak edge region.

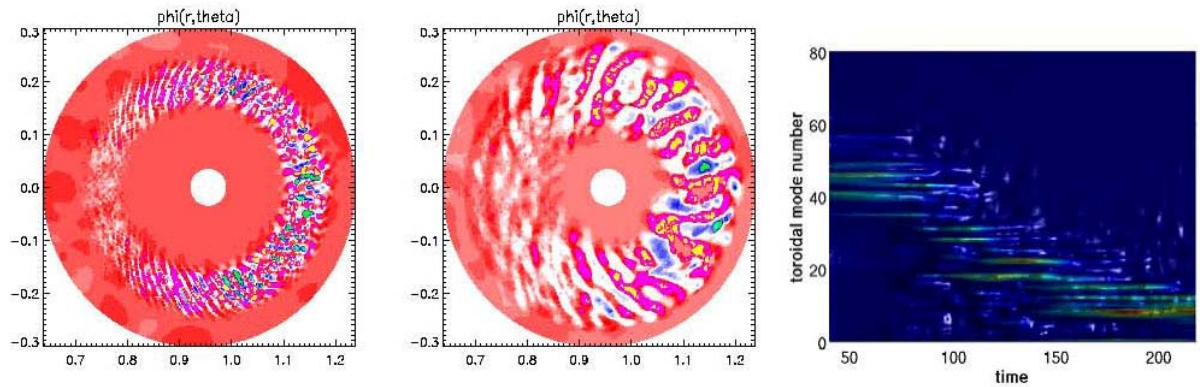

Figure 10. Contour plots of density fluctuations on a poloidal plane at t = 60 (left) and t = 160 (middle), and time evolution of toroidal spectrum $|\delta n_n|^2$ (right) in ∇T_e-driven CTEM turbulence, showing the generation of low-n, blob-like, large fluctuation structures.

6. Summary

State-of-the-art, first-principles-based global gyrokinetic simulations, which exploit leadership-class computational resources and cooperate with experimental and theoretical studies, are shown to lead to real advances in understanding some key physics issues in fusion science.

Specifically, global gyrokinetic simulations using the GTS code have discovered an important nonlinear flow generation process due to residual stress produced by micro-turbulence. The key results remarkably contribute to elucidating critical issues with regard to the origin of intrinsic rotation, underlying physics governing the experimental empirical laws of intrinsic rotation with respect to plasma gradients and current, and underlying dynamics governing the radial penetration of modulated flows in experiments. Simulations also have made important predictions in regimes where experiments can validate.

Acknowledgments

The authors would like to express thanks to Dr. L. Zakharov for generating numerical MHD equilibria using the ESC code for current scan simulations. Simulations were performed on Franklin at the National Energy Research Scientific Computing Center (NERSC) and on Jaguar/pf at the National Center for Computational Sciences (NCCS). This work was supported by U.S. DOE Contract No. DE-AC02-09CH11466 and the SciDAC project for Gyrokinetic Particle Simulation of Turbulent Transport in Burning Plasmas.

References

[1] J. E. Rice *et al*., Nucl. Fusion **44**, 379 (2004).
[2] J. E. Rice *et al*., Nucl. Fusion **47**, 1618 (2007).
[3] M. Yoshida *et al*., Phys. Rev. Lett. **100**, 105002 (2008).
[4] K. Ida *et al*., Nucl. Fusion **50**, 064007 (2010).

[5] S. D. Scott *et al*., Phys. Rev. Lett. **64**, 531 (1990).
[6] P. H. Diamond *et al*., Phys. Plasmas **15**, 012303 (2008).
[7] W. X. Wang *et al*., Phys. Plasmas **13**, 092505 (2006).
[8] W. X. Wang *et al*., Phys. Plasmas **13**, 092501 (2006).
[9] F. L. Hinton *et al*., Phys. Fluids **28**, 3082 (1985).
[10] I. Manuilskiy and W. W. Lee, Phys. Plasmas **7**, 1381 (2000).
[11] W. X. Wang *et al*., Phys. Plasmas **17**, 072511 (2010).
[12] W. X. Wang *et al*., Phys. Plasmas **14**, 072306 (2007).
[13] W. X. Wang *et al*., Phys. Rev. Lett. **102**, 035005 (2009).
[14] R. Dominguez and G. M. Staebler, Phys. Fluids, B **5**, 3876 (1993).
[15] O. D. Gurcan *et al*., Phys. Plasmas **14**, 042306 (2007).
[16] P. H. Diamond *et al*., Nucl. Fusion **49**, 045002 (2009).